Wireless Networks (2023) 29:3255–3270
https://doi.org/10.1007/s11276-023-03250-7

ORIGINALPAPER

Crown shaped edge multiband antenna design for 5G and X-Band applications

Baris Gurcan Hakanoglu[1] · Veli Tayfun Kilic[3] · Fatih Altindis[3] · Mustafa Turkmen[2,4,5]

Accepted: 18 January 2023 / Published online: 3 June 2023

Abstract

Nowadays we are experiencing the fifth-generation (5G) technology with new frequency bands to achieve high broadband speed, minimum latency and more developed end user devices. Due to the different frequency ranges for different applications at 5G bands the antennas should support multiband operation in a compact structure. This paper proposes a new multiband microstrip patch antenna design operating at mid band 5G frequencies and in the X band. The structure of the antenna includes simply loading the top radiating edge with rhombic shaped stubs and slots. This configuration yields the antenna to have resonances at multiple frequencies based on the fact that the stubs and slots affect capacitive and inductive impedances on the lower and higher operating frequencies of the antenna. The unique design enables the antenna to have reasonably high gains at four different bands of 6.76 dBi, 6.47 dBi, 7.76 dBi and 5.51 dBi at 3.34 GHz, 4.61 GHz, 6.01 and 8.02 GHz, respectively. Also, the simulated antenna has been manufactured and measured. The measurement results are in good agreement with the simulation results. The proposed design can be used with many other frequency bands and dielectric materials as well to achieve multiband operation.

Index Terms Microstrip patch antennas · Multiband operation · 5G mobile communication · Wireless networks

1 Introduction

Rapid advances in the evolution of new generation wireless communication systems raised a growing demand for multiband antennas. Operating at different bands by a single antenna is an efficient way due to the limited space that most modern electronic devices can allow for. Especially for the fifth generation (5G) technology applications antennas with multiband operation are required to be used because in operation massive number of devices have request to access to the 5G networks serving at different bands in various countries. In Europe 3600–3800 MHz frequency band has been allocated for the early phase development for 5G. On the other hand, Japan and China has planned to release 4400–5000 MHz band for 5G and United States opened up 3550–3700 MHz band for a new Citizens Broadband Radio Service [1]. Following the determination of the frequency bands many studies were performed to meet the frequency requirements of 5G network systems including single and multiband antenna designs. For example, the authors have focused on 3.4 – 3.8 GHz band with a hand-pump shape microstrip antenna in [2], whereas a triple band dual-polarized antenna that consists of two orthogonal dipole antennas

✉ Baris Gurcan Hakanoglu
bhakanoglu@bandirma.edu.tr

Veli Tayfun Kilic
tayfun.kilic@agu.edu.tr

Fatih Altindis
fatih.altindis@agu.edu.tr

Mustafa Turkmen
turkmen@erciyes.edu.tr

1 Department of Electrical-Electronics Engineering, Bandirma Onyedi Eylul University, 10200 Balikesir, Turkey

2 Department of Electrical - Electronics Engineering, Erciyes University Talas, 38039 Kayseri, Turkey

3 Department of Electrical and Electronics Engineering, Abdullah Gul University, Sumer Campus, 38080 Kayseri, Turkey

4 Fotonik Technology and Engineering, Erciyes Technopark Talas, 38039 Kayseri, Turkey

5 Nokta Detection Technologies R&D Center Sancaktepe, 34785 Istanbul, Turkey

each including three different radiator types has been proposed for 2G, 3G, 4G and sub-6 GHz 5G applications in [3]. Moreover, to realize dual operating bands in 5G frequencies inverted L-shaped slots are proposed for a microstrip antenna [4]. Similarly, dual-band operation has also been achieved by the antennas having 2 S shape with a compact structure [5].

Defected Ground Structure (DGS), in which etching slots are formed on the ground plane, is another method that yields antennas to operate on multiple frequency bands. Antennas with defected ground are proposed to be used for many wireless bands including WLAN/WiMAX (Wireless Local Area Networks/Worldwide Interoperability for Microwave Access), RFID (Radio Frequency Identification), GPS (Global Positioning System), X band, UWB (Ultra-Wideband) and 5G applications [6–18]. This is because of the fact that depending on the shapes and locations of the slots, resonance behavior of an antenna changes. In addition, it is worth noting that the reconfigurable antennas can also be used to achieve multiband operation [19–23]. However, in both methods for optimum multiband operation it is required to modify and optimize the ground or to determine appropriate electronic components with help of a parametric analysis that might be time consuming.

In this paper a design method based on changing effective capacitance and inductance of the antenna for multiband operation is proposed. The method includes loading the top edge of the antenna with rhombic shaped stubs and slots giving the antenna a crown shape. The design procedure is simpler than designing an EBG (Electromagnetic Band Gap) structure on the ground plane or placing electronic components on the antenna. With the proposed approach a multiband patch antenna was designed to be used for 5G networks and X band applications. Due to the stubs and slots on its patch the designed antenna radiates at four different bands that are around 3.34 GHz, 4.61 GHz, 6.01 and 8.02 GHz with gains of 6.76 dBi, 6.47 dBi, 7.76 dBi and 5.51 dBi, respectively. In addition, to verify the simulation results, a prototype antenna was fabricated and measurements were obtained. The measurement results are in very good agreement with the simulation results.

Table 1 Some of the characteristics of RT6002 [27]

	Typical Value	Units
Dielectric Constant	2.94 ± 0.04	-
Dissipation Factor	0.0012	-
Thermal Coefficient of ε_r	+12	ppm/°C
Volume Resistivity	10^6	MΩ*cm
Surface Resistivity	10^7	MΩ
Moisture Absorption	0.02	%
Density	2.1	gm/cm3
Copper peel	1.6	N/mm

2 Antenna design and simulation

The reference antenna is designed using RT6002 dielectric substrate with relative permittivity (ε_r) of 2.94, loss tangent of 0.0012 and thickness (h) of 1.524 mm. Width (W_{subs}) and length (L_{subs}) of the substrate are 56.40 mm and 44.34 mm, respectively. RT6002 is frequently used in microwave frequencies, especially with its low dielectric constant and low loss. Larger bandwidth and higher gain antennas can be designed with low dielectric constant materials. In addition, it can be used safely in both indoor and outdoor environments with its low thermal coefficient of 12 ppm/°C and an operating capacity between −55° and +125° degrees [27]. Moreover, by having excellent physical stability it is suitable for the proposed antenna, which has tight design points such that narrow etchings have to be performed on the radiating part. Because of these features RT6002 has been chosen for the design process. Some of the characteristics of RT6002 is shown in Table 1.

The proposed antenna geometry is shown in Fig. 1. As seen in the figure, the antenna has rectangular shape with patch width (W_{patch}) and length (L_{patch}) which dimensions were found according to the transmission line model [24]. The antenna is fed by a microstrip feed line and two notches exist along the two sides of the feeding line, whose length and width are presented with F_i and g, respectively. These notches in the designed antennas are formed based on inset feeding technique that is one of the most popular methods to excite an antenna enabling to set antenna resistance. The parameter F_i or the inset feeding distance affect the input resistance of the antenna at resonance which changes with the ratio of the length of the inset, F_i over the side length of the patch, L_{patch} as a function of $\cos^2(\pi\ Fi/L_{patch})$ [28]. So, when the inset-feed point is transferred from the radiating edge toward the center of the patch, i.e., when length of the inset becomes half of the side length of the patch, the antenna input impedance decreases to zero. That is the reason why length of the inset in a rectangular patch antenna is chosen smaller than half of the antenna length. On the other hand, the parameter g or the width of inset feeding affects mainly the bandwidth of the antenna. An equation has been proposed for the relation of the width of the inset feeding and the width of the patch [28]. According to this equation when the width of the inset feeding is decreased from $W_{patch}/10$ to $W_{patch}/40$ the bandwidth of the antenna is increased by 46.2%. Also, there was a small shift with the resonant frequency of 0.06 GHz. In order to understand the contribution of the inset feeding technique to the antenna in more details, the circuit equivalent model of the rectangular patch antenna must first be considered. In this model, the antenna can be shown as two radiating slots, each with a width of W_{patch} and a height of h, located at a distance of

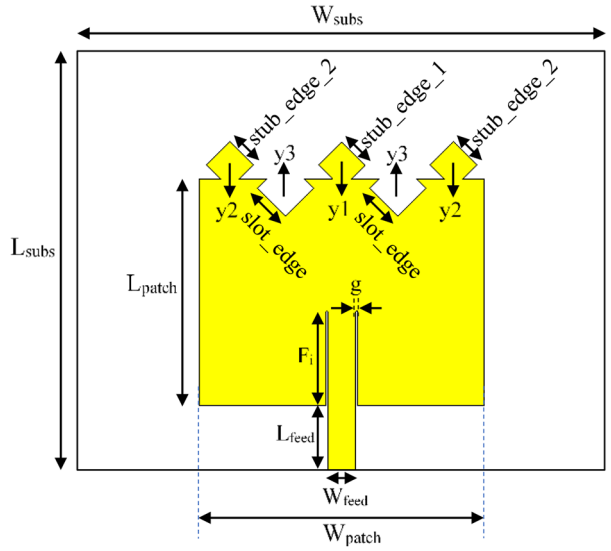

Fig. 1 Top view of the proposed patch antenna loaded with the configuration of rhombic shaped stubs and slots

Table 2 Optimized parameters of the proposed antenna

Parameter	Value (mm)	Parameter	Value (mm)
W_{patch}	30.51	stub_edge_1	3.54
L_{patch}	24.39	stub_edge_2	3.54
W_{subs}	56.40	slot_edge	4.24
L_{subs}	44.34	y_1	1.00
W_{feed}	3.00	y_2	1.00
L_{feed}	7.00	y_3	2.00
F_i	10.15	h	1.52
g	0.17	ε_r	2.94

L_{patch} from each other. Each slot is equal to parallel equivalent admittance Y and susceptance B at conductivity G. The effect of a single slot in terms of conductance and mutual conductance can be calculated using Eqs. 1 and 2 [28, 29];

$$G_1 = \frac{1}{120\pi^2}\int_0^{\pi}\left[\frac{\sin\left(\frac{k_0 W_{patch}}{2}cos\theta\right)}{cos\theta}\right]^2 sin^3\theta d\theta \tag{1}$$

$$G_{12} = \frac{1}{120\pi^2}\int_0^{\pi}\left[\frac{\sin\left(\frac{k_0 W_{patch}}{2}cos\theta\right)}{cos\theta}\right]^2 * J_0\left(k_0 L_{patch} sin\theta\right) sin^3\theta d\theta \tag{2}$$

where G_1 and G_{12} are the self-conductance and mutual conductance, respectively. Also, in the equations J_0 is the Bessel function of the first kind of order zero and k_0 represents the wavenumber in patch antenna along the E- and H-planes. Finally, by taking the mutual effects into the analysis resonant input impedance can be calculated using the Eq. 3, where R_{in} is the antenna's resonant input impedance [29].

$$R_{in} = \frac{1}{2\left(G_1 + G_{12}\right)} \tag{3}$$

In Fig. 1, feed line length (L_{feed}) and width (W_{feed}) are illustrated, too. In the design of crown shaped edge, the rhombic shaped stubs and slots are first formed to have their corner points on the edge of the radiating patch and then shifted towards outside and inside of the patch, respectively. In Fig. 1, the distance how much the centre stub gets into the radiating patch in y-direction is pointed out with parameter y_1. Also, the distance how much the stubs at left and right get into the patch is represented with y_2. On the other hand, the outrun of the slots from the patch is indicated with y_3. In the figure, the side lengths of the stubs are denoted with stub_edge_1 and stub_edge_2 for the center stub and the stubs positioned in the left and right of the center stub, respectively. Similarly, side length of the slots between the stubs is represented with slot_edge.

The dimensions and positions of the stubs and slots together with their numbers play great role on the antenna characteristics. Therefore, detailed parametric analyses have been performed for different dimensions and coordinate values. The values of final design parameters of the proposed antenna obtained after parametric studies are given in Table 2 in coherence with the labels exist in Fig. 1.

The design method for the proposed antenna includes four steps that are given below. In addition, the antenna structures obtained in each step are shown in Fig. 2;

i. The reference antenna design, Ant.#1,
ii. Loading the reference antenna with one stub, Ant.#2,
iii. Loading Ant.#2 with two additional stubs, Ant.#3,
iv. Etching slots between the stubs, Ant.#4.

Figure 3a-e show the equivalent circuit models of traditional patch antenna, inset fed patch antenna, proposed antenna with one stub, proposed antenna with three stubs and proposed antenna with three stubs and two slots, respectively. The ordinary patch antenna can be modelled as a parallel RLC resonance circuit based on the cavity model presented in Fig. 3a [30]. When inset feeding is applied to the antenna, two slots are introduced and the current should flow around these slots which in turn yields adding a series inductance ΔL_p and capacitance ΔC_p to the equivalent circuit of the antenna constituting two resonators as shown in Fig. 3b. In the equivalent circuit of the inset fed antenna C_{c1} presents the coupling capacitor between two resonators. When the antenna is loaded with a stub on the top radiating edge, the effect is adding inductive impedance at higher frequencies and capacitive impedance at lower frequencies [12]. These effects can be shown with adding to the equivalent circuit ΔL_{p2} and ΔC_{p2} as presented in Fig. 3c. Loading the antenna

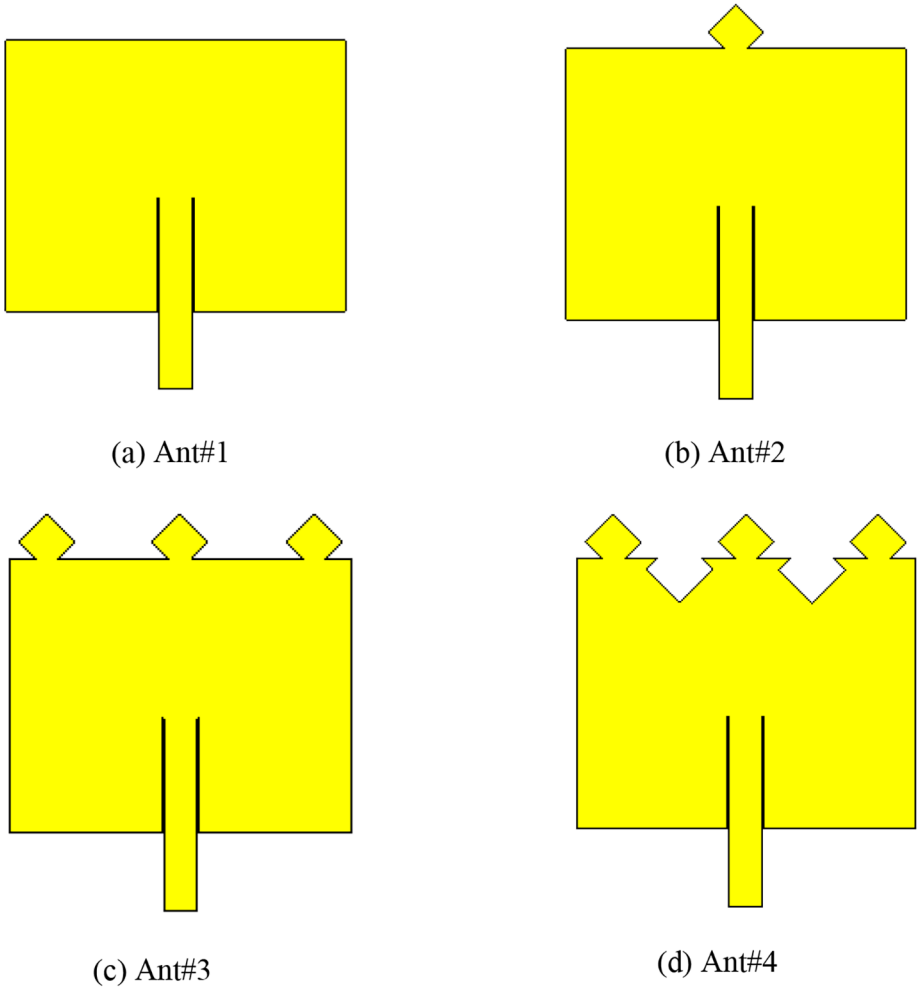

Fig. 2 Antenna structures designed in each step till proposed architecture

with two additional stubs introduces a new RLC resonator to the circuit with coupling capacitor C_{c2} shown in Fig. 3d [31]. Because of this coupling effect and altering the edge impedance of the antenna return loss levels for the second and fourth bands are very close to limit level which is -10 dB. In addition, the second resonance frequency is not at the desired point. Hence a pair of rhombic shaped slots are etched between the stubs all symmetrically placed to solve the mentioned problems. These slots will add a new RLC resonator circuit to the equivalent model with a coupling capacitor C_{c3}. The value of the coupling capacitors, C_{c2} and C_{c3}, can be ignored because their value is much lower than the equivalent value of the third and fourth RLC circuit [12]. Consequently, the latest equivalent circuit is the same as it was in the model with the inset feed shown in Fig. 3b with different inductance and capacitance values.

To obtain a mathematical expression of the proposed model the equivalent impedance of the circuit shown in Fig. 3e has been presented. For simplicity, each RLC resonator is denoted by the letter Z. Here;

$$Z_1 = R_{p1} \parallel (jwL_{p1} + jw\Delta L_{p1}) \parallel \frac{1}{\frac{1}{jwC_{p1}} + \frac{1}{jw\Delta C_{p1}}} \tag{4}$$

$$Z_2 = R_{p2} \parallel (jwL_{p2} + jw\Delta L_{p2}) \parallel \frac{1}{\frac{1}{jwC_{p2}} + \frac{1}{jw\Delta C_{p2}}} \tag{5}$$

$$Z_3 = R_{p3} \parallel jwL_{p3} \parallel \frac{1}{jwC_{p3}} \tag{6}$$

$$Z_4 = R_{p4} \parallel jwL_{p4} \parallel \frac{1}{jwC_{p4}} \tag{7}$$

The equivalent impedance of the whole circuit can be written as follows;

$$\left\{\left[\left[\left[\left(Z_4 + \frac{1}{jwC_{c3}}\right) \parallel Z_3\right] + \frac{1}{jwC_{c2}}\right] \parallel Z_2\right] + \frac{1}{jwC_{c1}}\right\} \parallel Z_1 \tag{8}$$

In the design, as the first step the reference antenna denoted by Ant.#1 is formed to operate at 3.5 GHz. The designed

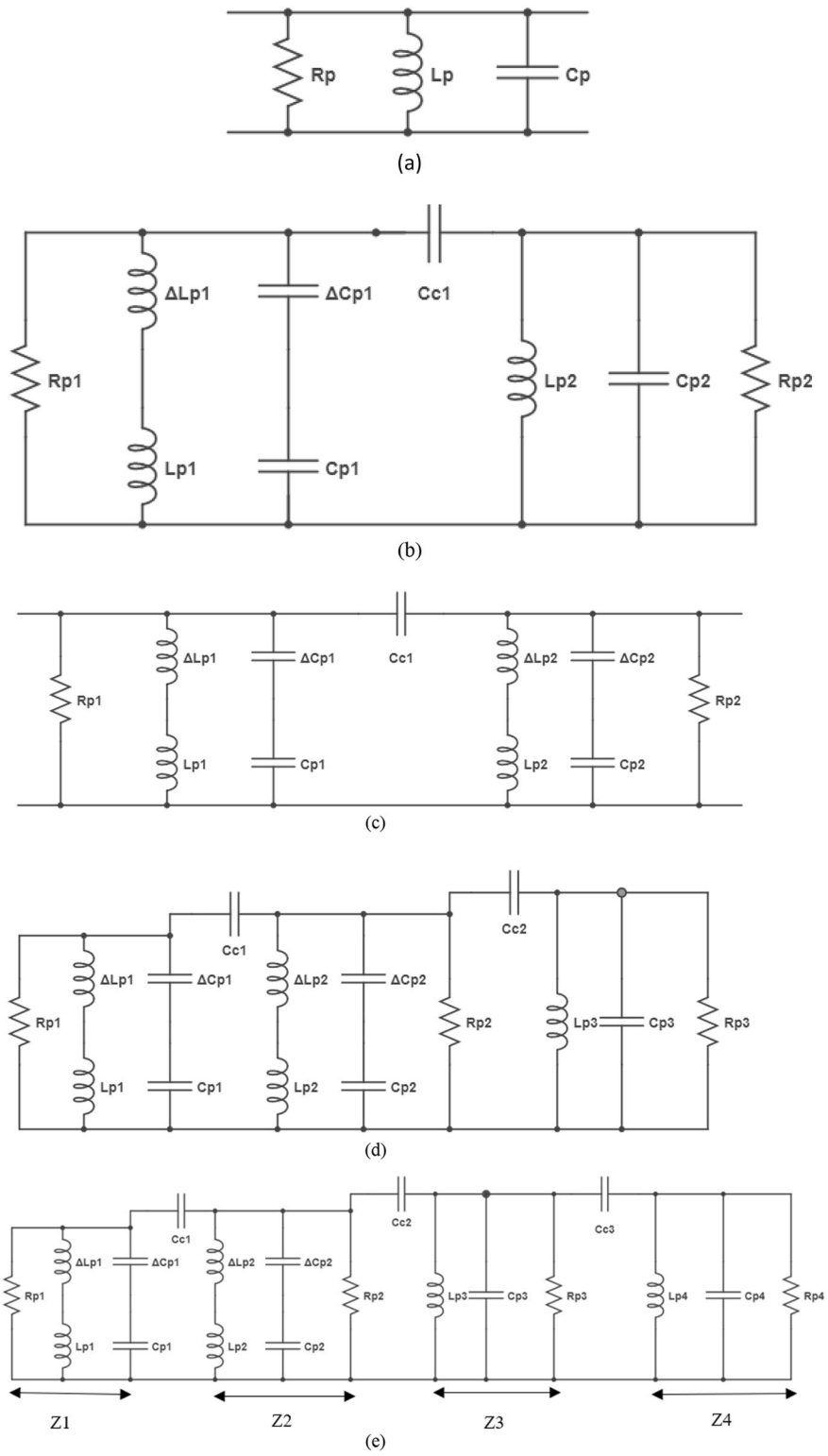

Fig. 3 Equivalent circuit of design steps of the antenna, (a) Conventional patch, (b) Inset fed patch, (c) Inset fed patch with a tuning stub, (d) Inset fed patch with two additional tuning stubs, (e) Inset fed patch with three tuning stubs and two slots

antenna was simulated with three-dimensional (3D) simulation tool [25]. S_{11} parameter change with frequency calculated in simulations for the reference antenna, Ant.#1, is shown in Fig. 4 with black line. As seen in the figure the antenna has three resonances at which S_{11} value is below − 10 dB.

The first resonance at 3.5 GHz corresponds to the fundamental TM_{10} mode and the other resonances at 5.64 and

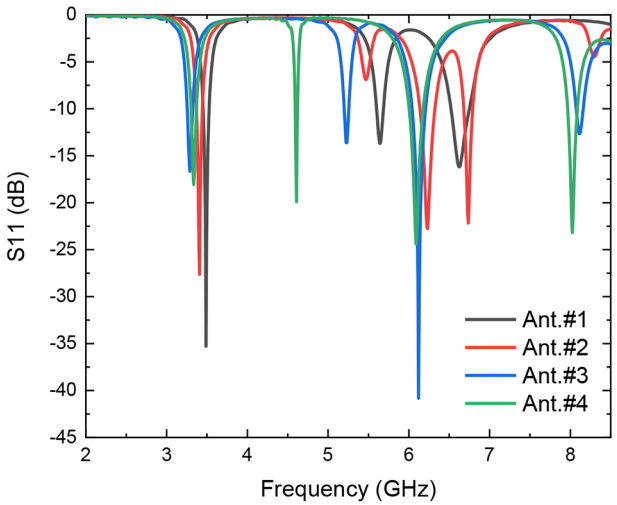

Fig. 4 Variation of S_{11} parameter magnitude with frequency calculated for the antenna designs, Ant.#1, Ant.#2, Ant.#3, and Ant.#4

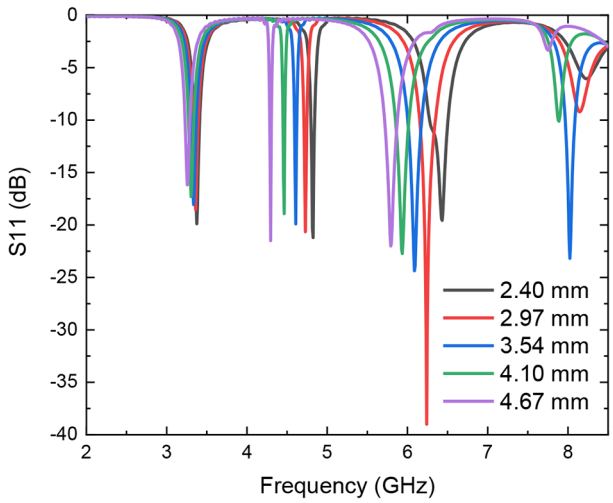

Fig. 5 S_{11} parameter magnitude change with frequency calculated for the proposed antenna design, Ant.#4, with the center stub having different edge lengths, stub_edge_1

6.62 GHz correspond to higher order modes. Next, the first open circuit stub that is at the center is loaded to the reference antenna. The new antenna is called Ant.#2. As for the reference antenna, S_{11} parameter change of Ant.#2 with frequency was calculated in 3D simulations. The result is shown in Fig. 4 with red line. As seen in the figure, three resonances arise for the antenna at 3.41 GHz, 6.23 and 6.75 GHz with S_{11} value lower than − 10 dB. However, the resonance frequencies obtained with Ant.#2 are not at the desired bands. Therefore, these operating bands should be tuned to achieve the operation at mid 5G and X bands. For this purpose, additional stubs have been added symmetrically to the two sides of the center stub which forms the antenna denoted by Ant.#3. Because the center stub contributes to the capacitive impedance at lower frequency bands and inductive impedance at higher frequency bands [26] loading the antenna with additional stubs having the same shape with the center stub enhances the capacitive and inductive impedance effects of the center stub [12]. In addition to altering the matched impedance of the antenna at the pass band frequencies, adding these stubs also causes changes in capacitance due to the coupling capacitance between them and center stub [12]. As for the previous designs, detailed parametric analyses were performed for the antenna with help of 3D simulations. S_{11} parameter change of the designed antenna having three stubs, i.e., Ant.#3, is shown in Fig. 4 with blue line. In the figure, it is seen that the resonances arise almost at the desired frequencies. However, due to the coupling effect between the stubs and impedance matching disturbance S_{11} levels for the second and fourth resonance frequencies are very close to -10 dB. In addition, the second resonance frequency is far from the desired point. To overcome these problems a pair of rhombic shaped slots are etched between the stubs all symmetrically placed. The final antenna design with three stubs and two slots between them is named Ant.#4. Thanks to its unique geometry the antenna enables increased current path at the slot edges that results in resonance frequencies shift to lower frequencies with respect to previous designs. Therefore, with the last antenna design, i.e., Ant.#4, four resonances arise in the required frequency bands. As for the other antennas, frequency response of Ant.#4 was calculated, too, with simulations. S_{11} variation with frequency for Ant.#4 is shown in Fig. 4 with green line. It is clearly seen that the designed antenna has four resonances with S_{11} values far below − 10 dB in the desired frequency bands.

As seen in Fig. 1 there are many geometrical parameters that affect the antenna performance. To understand performance change of the antenna with these design parameters, analyses were done for different parameter values. In conducted studies only a single parameter is changed in each analysis. These analyses and the results are explained further in the following subsections.

2.1 Performance analyses of the stubs

In the designs, initially the centre stub with various lengths is placed on the top edge of the patch and it is shifted towards the patch parametrically until the optimum design is achieved. First, edge length (stub_edge_1) and shifting distance (y_1) of the centre stub were changed and analyses were performed. Change of S_{11} parameter magnitude with frequency for the designed antenna is shown in Figs. 5 and 6 for various edge lengths and shifting distances of the centre stub, respectively. As seen in the figures, resonances in all bands shift continuously to lower frequency ranges as

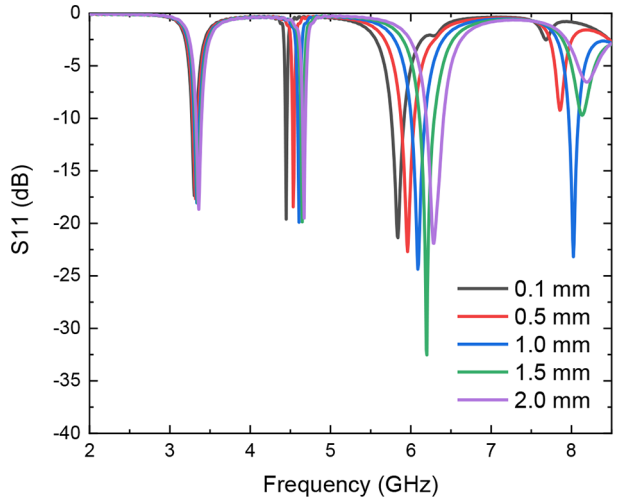

Fig. 6 S_{11} parameter magnitude change with frequency calculated for the proposed antenna design, Ant.#4, with the center stub having different shifting distances, y_1

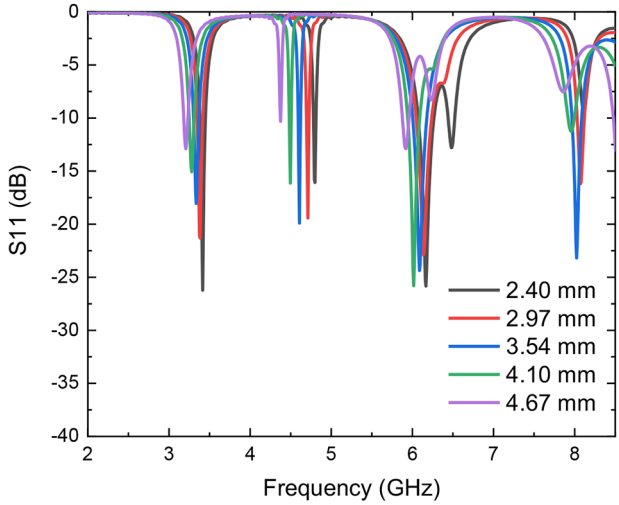

Fig. 7 S_{11} parameter magnitude change with frequency calculated for the proposed antenna design, Ant.#4, with the outer stubs having different edge lengths, stub_edge_2

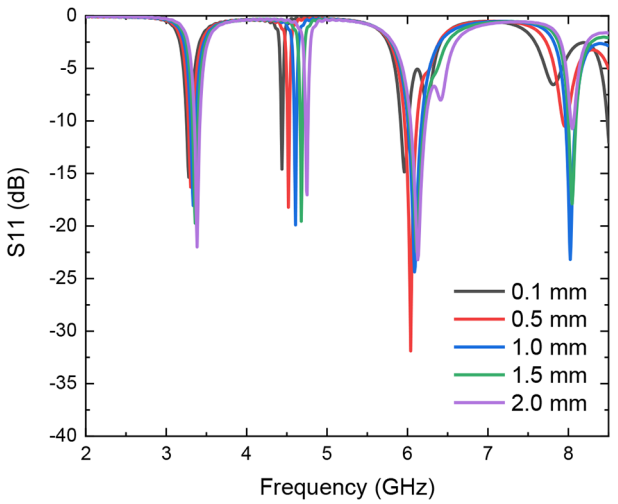

Fig. 8 S_{11} parameter magnitude change with frequency calculated for the proposed antenna design, Ant.#4, with the outer stubs having different shifting distances, y_2

the stub edge length increases, whereas resonances shift to higher frequency ranges with the increase of shifting distance. However, frequency range shifting in the second and third resonances that are around 4.5 and 6 GHz, respectively, are much more than that obtained in the first resonance that is around 3.5 GHz.

On the other hand, in the figures it is also seen that the fourth resonance is more sensitive to the changes in the parameters. Among the five different edge lengths and five different shifting distances that were considered in the analyses, S_{11} parameter is found to be below − 10 dB only for the cases of 3.54 mm edge length and 1.0 mm shifting distance at fourth resonance frequency. Moreover, it is important to note that for the designed antenna by changing the stub edge length the resonance frequencies can be set to a range between 4.3 and 4.8 GHz and 5.8 – 6.4 GHz for the second and third resonances, respectively. Similarly, with the change of stub shifting distance the second and third resonances can be tuned between 4.5 and 4.7 GHz and 5.8 – 6.3 GHz, respectively.

Next, analyses were repeated for the designed antenna, Ant.#4, with various edge lengths (stub_edge_2) and shifting distances (y_2) of the stubs placed on the right and left side of the centre stub. In the designed antenna, distance between the centre stub and the outer stubs are set to be the same. In other words, the stubs at the left and right are symmetrically placed with respect to centre stub at the middle. As in parametric analyses performed for the centre stub, simulations were first obtained for the antenna with the outer stubs having various edge lengths placed on the top side of the patch and then these stubs were shifted towards the patch continuously. S_{11} magnitude change with frequency calculated in the simulations for the designed antenna with the outer stubs having various edge lengths and shifting distances are shown in Figs. 7 and 8, respectively. As in the centre stub analyses, in the figures it is seen that the resonance frequencies in all the resonances shift to lower frequency ranges as the edge length of the stubs gets longer. However, resonance frequencies shift to higher frequency bands as the shifting distance increases. In addition, it is also seen that resonance frequency shifts are stronger for the second and third resonances than those obtained for the first and fourth resonances. For the designed antenna by changing the edge length of the outer stubs the second and third resonance frequencies of the antenna are adjusted to

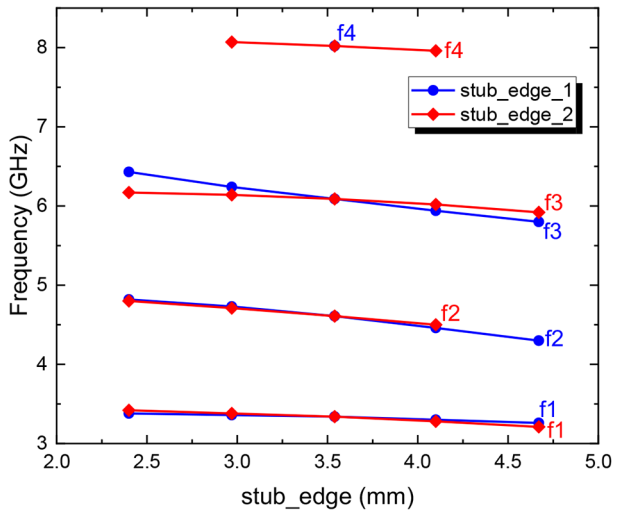

Fig. 9 Resonance frequency changes with edge lengths of the center (stub_edge_1) and outer stubs (stub_edge_2) in the proposed antenna design, Ant.#4

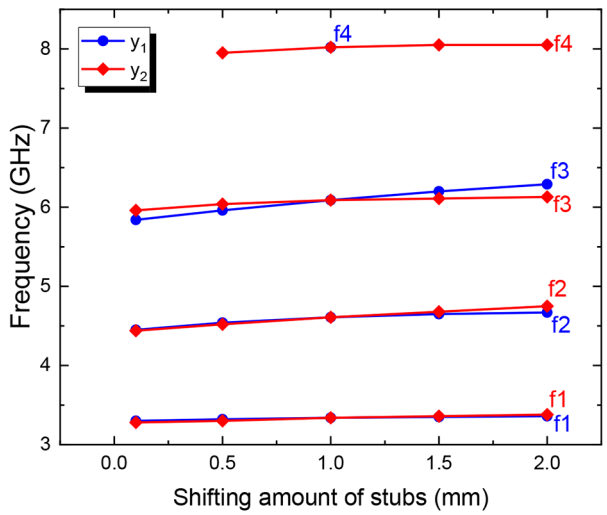

Fig. 10 Resonance frequency changes with shifting distances of the centre (y1) and outer stubs (y2) in the proposed antenna design, Ant.#4

be between 4.4 and 4.8 GHz and 5.9 – 6.2 GHz, respectively. These ranges are narrower than those obtained for the designed antenna by changing the edge length of the centre stub. On the other hand, for the designed antenna by altering the shifting distance of the outer stubs the second and third resonance frequencies are tuned between 4.4 and 4.8 GHz and 6.0 – 6.1 GHz, respectively.

If one compares it is seen that the second resonance frequency tuning range obtained for the designed antenna by varying the shifting distance of the outer stubs is wider than that obtained for the antenna by varying the shifting distance of the centre stub. On the contrary, the third resonance frequency tuning range obtained for the antenna by changing

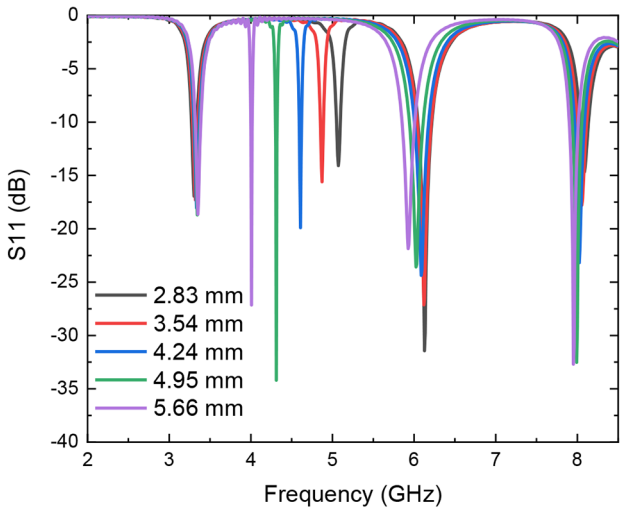

Fig. 11 S_{11} parameter magnitude change with frequency calculated for the proposed antenna design, Ant.#4, with the slots having different edge lengths, slot_edge

the shifting distance of the outer stubs is narrower than that found for the antenna by changing the shifting distance of the centre stub. These comparisons can be more easily done in Figs. 9 and 10, where variations of the resonance frequencies for the designed antenna with edge lengths of the stubs and their shifting distances are illustrated, respectively. In the figures, the first, second, third, and fourth resonance frequencies are labelled as f1, f2, f3, and f4, respectively.

Moreover, it is important to note that in the outer stub edge length and shifting distance parameter analyses of the designed antenna S_{11} parameter is found to be below −10 dB at fourth resonance frequency for three different stub edge lengths and four different shifting distances, whereas in the centre stub edge length and shifting distance parameter analyses of the antenna it was achieved only for a single edge length and shifting distance.

2.2 Performance analyses of the slots

As for the edge length and shifting distance of the stubs, performance analyses were performed for the designed antenna, Ant.#4, for five different values of the edge length and shifting distance of the slots. Change of S_{11} parameter magnitude with frequency for the designed antenna having different slot edge lengths and shifting distances are presented in Figs. 11 and 12, respectively.

In Figs. 11 and 12, it is seen that the main effect of slot edge and shifting distance change is on the return loss levels except for the second band. The effect on the second band is seen as frequency shifting to higher and lower bands.

The second resonance frequency can be set to a value between 4.01 and 5.07 GHz by changing the length from

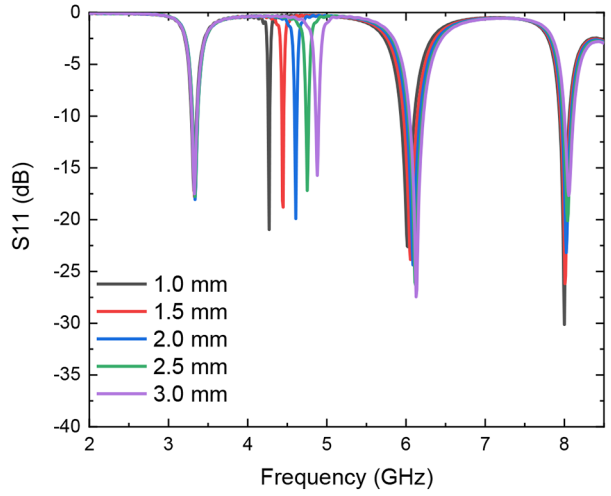

Fig. 12 S_{11} parameter magnitude change with frequency calculated for the proposed antenna design, Ant.#4, with the slots having different shifting distances, y_3

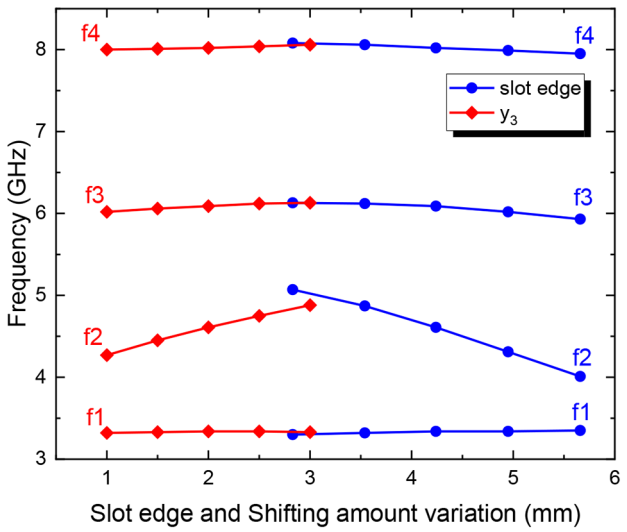

Fig. 13 Resonance frequency changes with edge lengths (slot edge) and shifting distances (y_3) of the slots in the proposed antenna design, Ant.#4

5.66 mm to 2.83 mm and between 4.27 and 4.88 GHz by changing the shifting distance from 1 to 3 mm. These resonance frequency changes are clearly seen in Fig. 13. In the figure, the first, second, third, and fourth resonance frequencies are labelled as f1, f2, f3, and f4, respectively.

3 Results and discussion

To verify the calculated results the designed antenna was fabricated and measurements were obtained. Photo of the fabricated antenna from top and bottom views is illustrated in Fig. 14a and b. As in the design, the antenna was manufactured on a pcb consists of the dielectric substrate RT6002 having a thickness of 1.524 mm and sandwiched between two copper layers with thickness of 0.035 mm. Also, geometry of the antenna is the same with that of the antennas simulated such that in the manufactured antenna patch width and length are 30.51 mm and 24.39 mm, respectively, and substrate width and length are 56.40 mm and 44.34 mm, respectively. In addition, a 50 Ω SMA connector is installed to the end of microstrip feed line which has a width of 3 mm and length of 7 mm. The ground plane, on the other hand, completely covers the back of the substrate without any modification on it.

After manufacturing the designed antenna, S-parameter measurements were obtained with help of a vector network analyser. The measurement setup built in during experiments is shown in Fig. 15. In the setup the antenna under test is connected to the first port of the network analyser.

Measured S_{11} parameter over the frequency range of 2–10 GHz is shown in Fig. 16 together with the S_{11} parameter change calculated in the simulations. As seen in the figure, the measurement results are in good agreement with the simulation results. In the measurements four resonances occur at 3.41 GHz, 4.75 GHz, 6.26 GHz, and 8.19 GHz with −10 dB bandwidths of 40 MHz, 30 MHz, 200 MHz, and 100 MHz correspond to 1.17%, 0.63%, 3.20%, and 1.22% percentage bandwidths, respectively. The results show that the manufactured antenna resonates with only a few shifts compared to the calculated resonance frequencies that are 3.34 GHz, 4.61 GHz, 6.01 and 8.02 GHz, respectively.

Furthermore, gain of the designed antenna was calculated over the frequency band spanning from 2 GHz to 10 GHz. Result is shown in Fig. 17. In the figure it is seen that with the designed antenna peak gain values of 6.76 dBi, 6.47 dBi, 7.76 dBi and 5.51 dBi are achieved at four resonance frequencies of 3.34 GHz, 4.61 GHz, 6.01 and 8.02 GHz, respectively. In the figure, it is also seen that the gain has a tendency to increase with the frequency.

Surface current distribution of the antenna is calculated. In Fig. 18 surface current distribution of the antenna over the radiating patch at four antenna resonance frequencies is depicted. In the figure, it is seen that for all operating bands and at all resonance frequencies the current flow is concentrated around the stubs and slots much more than other sections of the antenna. Therefore, it can be interpreted that thanks to the proposed method multi-band operation is achieved by enabling electromagnetic energy to be concentrated on a larger surface on the radiating edge of the antenna.

Far-field radiation patterns for each resonant frequency calculated in the simulations are shown in Fig. 19a-d. Main lobe directions for each frequency are 2°, 123°, 45° and 32°

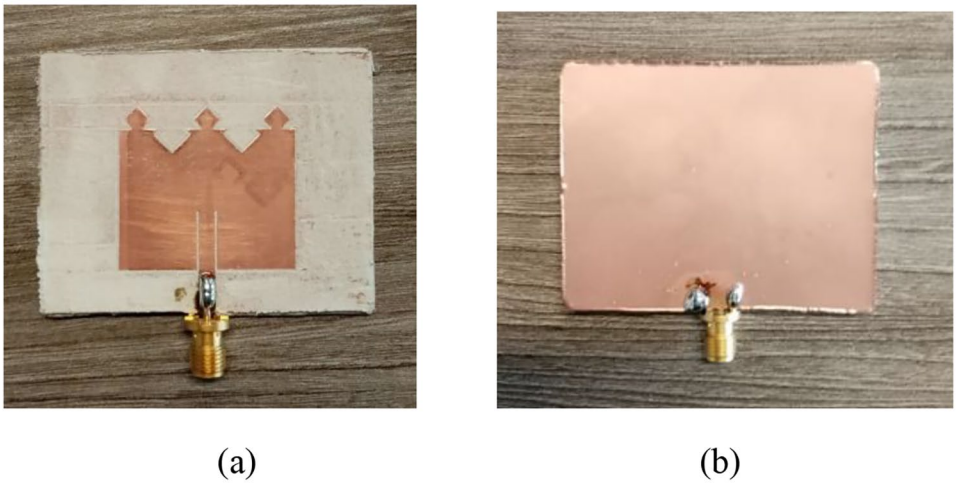

Fig. 14 Photo of the fabricated antenna from (a) top view and (b) bottom view

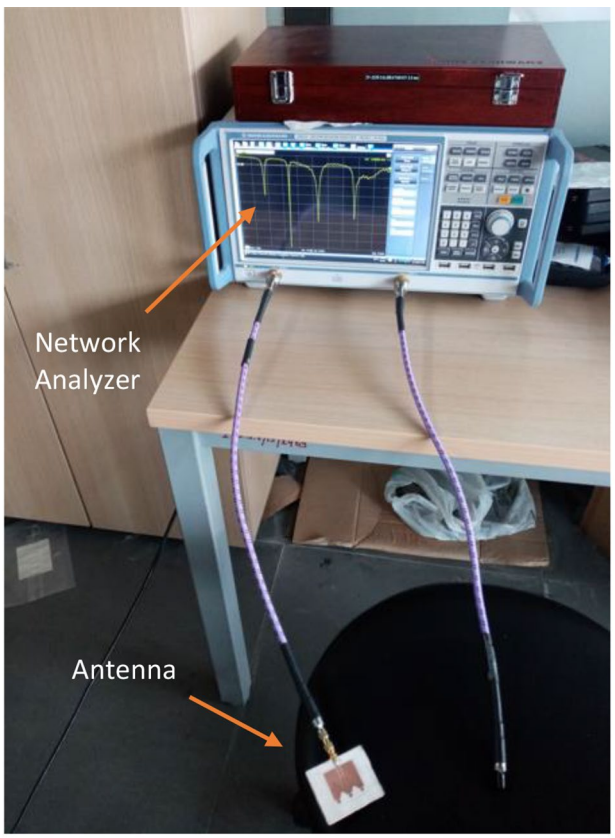

Fig. 15 Measurement setup with the antenna under test and the network analyser constructed during experiments

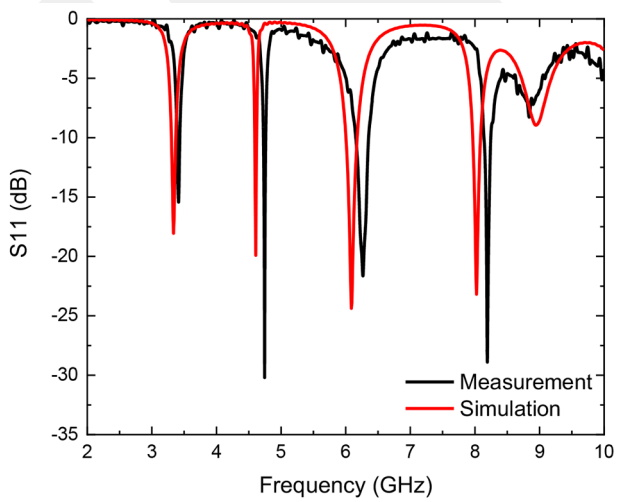

Fig. 16 Change of S_{11} parameter magnitude with frequency found in measurements and calculated in simulations

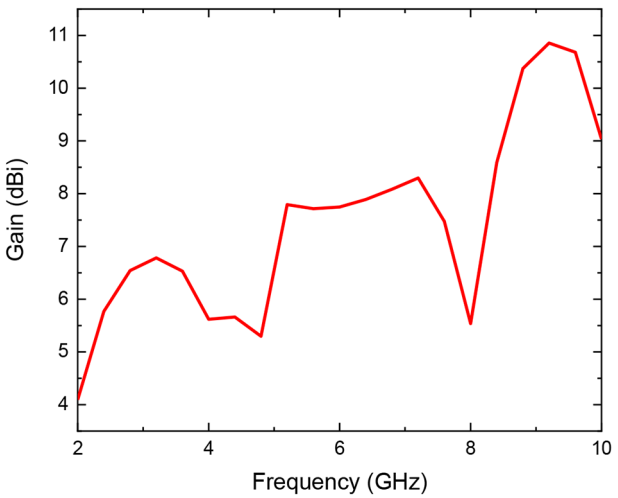

Fig. 17 Peak gain variation with frequency calculated for the designed antenna

at 3.34 GHz, 4.61 GHz, 6.01 and 8.02 GHz, respectively. In addition 3 dB angular width for 3.34 GHz, 4.61 GHz, 6.01 and 8.02 GHz are 88.5°, 62.1°, 56.5° and 73.3°,respectively.

For the designed antenna, characteristic mode analysis is performed with the help of computer simulation software in order to understand how much is the contribution of each mode at each resonance frequency. Thanks to

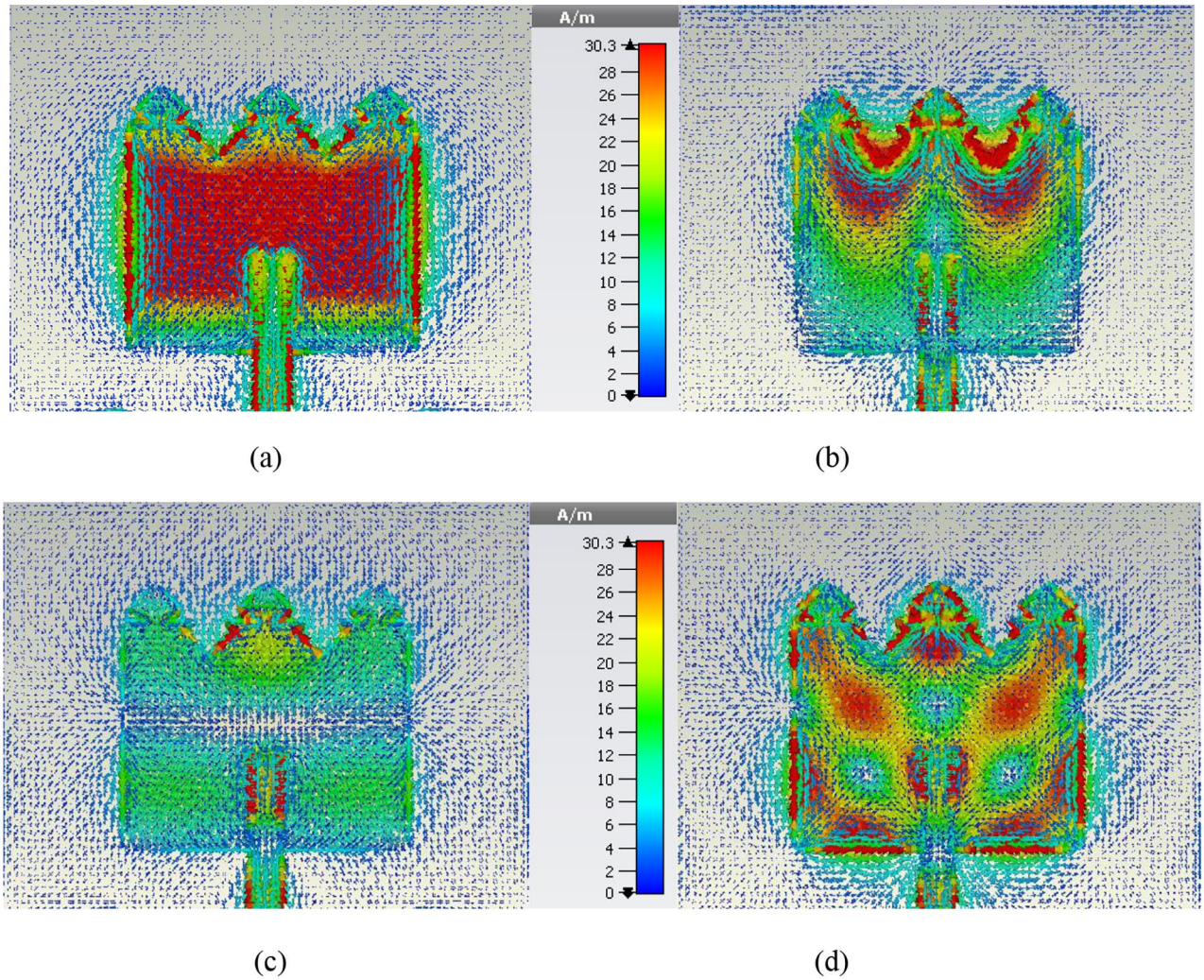

Fig. 18 Surface current distribution calculated for the designed antenna at resonance frequency of (a) 3.34 GHz, (b) 4.61 GHz, (c) 6.09 GHz, (d) 8.02 GHz.

the characteristic mode analysis, physical solution of an antenna with any geometry can be executed. In this way, the optimization and synthesis of antennas are examined in a simpler way. This analysis can be done by solving the generalized eigenvalue problem involving a set of orthogonal eigen currents and their associated eigenvalues with the impedance matrix of the moment method. The total current at the conductor surface can be expanded in modes due to the orthogonality of the eigen currents. The eigenvalues provide information about the radiating mode of the relevant band. In addition, modal significance MS_n and characteristic angles α_n can be calculated to express mode behaviours. [25]. These values depend on the eigenvalue λ_n as follows;

$$MS_n = \frac{1}{\sqrt{1 + |\lambda_n|^2}} \tag{9}$$

$$\alpha_n = 180^{\circ} - arctan\,(\lambda_n) \tag{10}$$

Modal significance of the first four modes calculated for the designed antenna over the frequency band between 2 and 8 GHz is shown in Fig. 20. As can be seen for all four resonances the modal significance values are very close to 1 for mode 1, mode 2, mode 3 and mode 4 at 3.34 GHz, 4.61 GHz, 6.01 and 8.02 GHz, respectively. More specifically, at the first resonance frequency of 3.34 GHz modal significance values of the first and second modes are of 0.99 and of 0.98, respectively. In addition, modal significance values of the third and fourth modes at the first resonance frequency of 3.34 GHz are of 0.84 and of 0.70, respectively. It shows that mode 1 and mode 2 are strongly present at the first resonance of the antenna but the contributions of mode 3 and mode 4 are weak.

On the contrary at 4.61 GHz all four modes have close contributions to the antenna resonance such as mode 1 has a

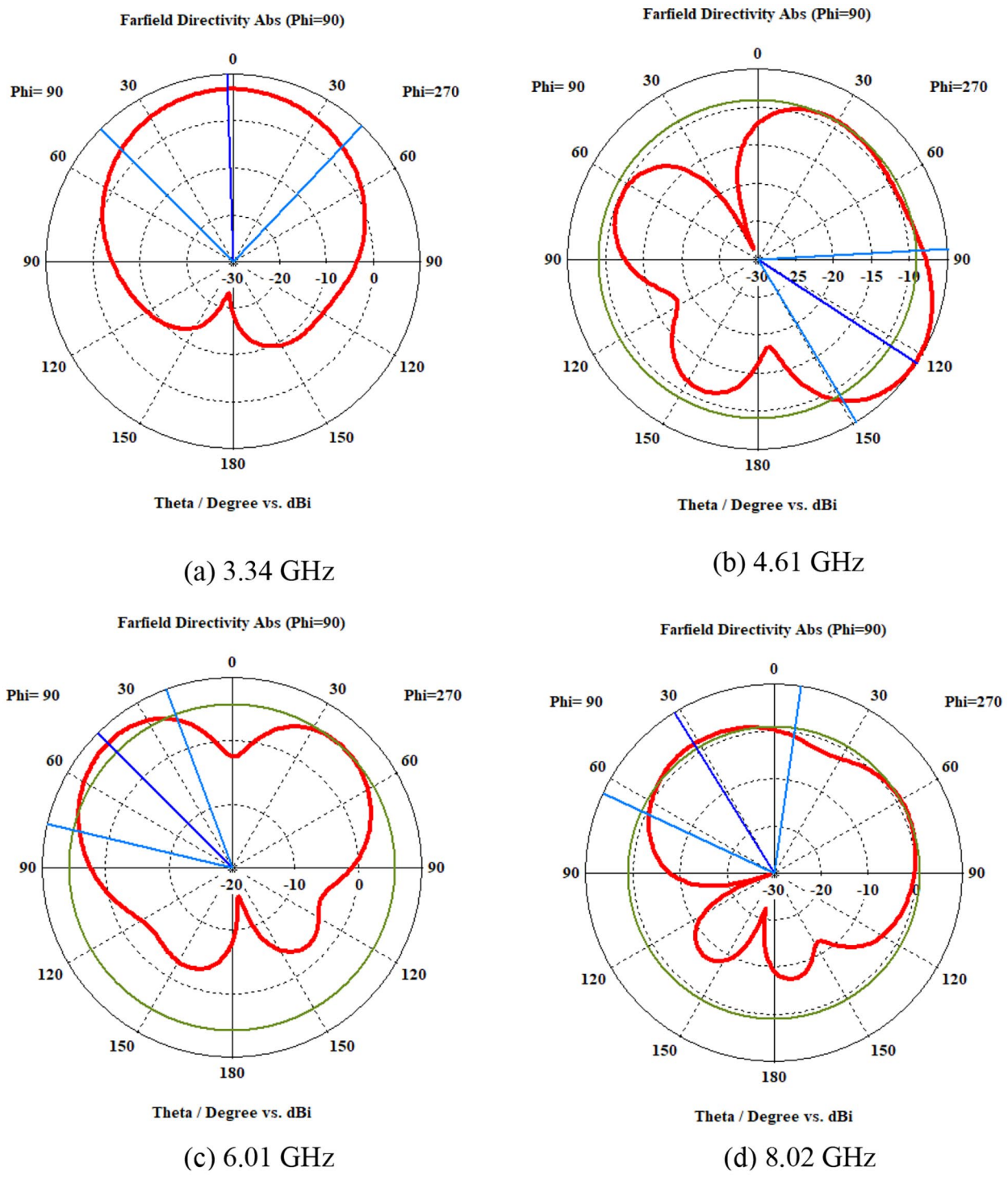

Fig. 19 Far field radiation patterns calculated for the designed antenna at resonance frequency of (a) 3.34 GHz, (b) 4.61 GHz, (c) 6.01 GHz, (d) 8.02 GHz.

significance value of 0.96, mode 2 has a significance value of 0.98, mode 3 has a significance value of 0.95 and mode 4 has a significance value of 0.99. Moreover, when we analyze the modes at 6.01 GHz, it is clear that mode 1, mode 3 and mode 4 provide the main contribution all with the significance value of 0.99. Besides at 6.01 GHz mode 2 has the significance value of 0.96. Finally at 8.02 GHz it is seen from the figure that all four modes strongly contribute to the fourth resonance of the antenna all with the significance value of 0.99.

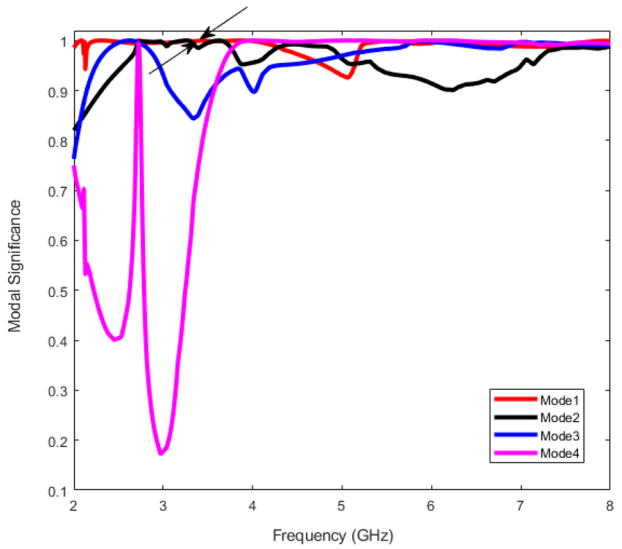

Fig. 20 Modal significance of the first four modes calculated for the designed antenna over the frequency band between 2 and 8 GHz.

The designed antenna is compared with the proposed multiband antennas exist in literature in Table 3 in terms of overall antenna sizes, resonance frequencies and peak gains at resonance frequencies. In the table, it is seen that the designed antenna, despite its smaller or comparable sizes, resonates at four frequencies that is more than the resonance frequency number of the other antennas listed in the table. Only the antenna reported in work [14] has four resonances as with our proposed antenna. However, peak gain values achieved at resonance frequencies with our designed antenna are considerably higher than those achieved not only with the antenna reported in that literature study but also with the other antennas exist in the table. In addition to all these properties, as it has been stated the main advantage of the proposed antenna is its simple design. In the proposed antenna architecture, there is no need to modify the ground plane, etching complex slots on the radiating part or adding electronic components. The proposed antenna structure can also be implemented on different pcb substrates with high dielectric constant to further reduce antenna sizes.

Table 3 Comparison of present work with the literature

Ref.	Description	Overall Size (mm^3)	Frequency Range (GHz)	Peak Gain (dB / dBi)
[4]	Dual-band 5G antenna with symmetrical L-shaped slots and partial ground plane	32×20×1.6	3.5 4.9	2.31 dB 3.88 dB
[5]	2 S shaped multiband patch antenna	20×15×1.6	5.6 11.5 12.7	2.09 dBi 5.8 dBi 5.7 dBi
[6]	Triple-band antenna with defected ground	38×25×1.59	2.61 3.5 5.4	1.85 dBi 2.19 dBi 0.26 dBi
[12]	DGS dual band antenna loaded with stubs and slots	33.5×33.5×1.52	3.532 6.835	4.02 dB 3.38 dB
[14]	Multiband planar antenna based on multiple resonant stubs	43×33×1.6	2.45 2.8 3.8 5.5	5.5 dBi 4.4 dBi 0.0 dBi 5.6 dBi
[15]	High gain triple band antenna with two slits and a T-shaped slot	47×37×1.6	4.17 5.80	7 dBi -
[19]	Reconfigurable multiband antenna	90×25×1.6	0.89 1.22 2.46	2 dBi 2.06 dBi 3.29 dBi
proposed	Multiband antenna loaded with stubs and slots	56.4×44.3×1.5	3.34 4.61 6.01 8.02	6.76 dBi 6.47 dBi 7.76 dBi 5.51 dBi

4 Conclusion

This paper proposes a novel multiband antenna design for mid band 5G and X band applications. The model includes a crown shaped edge that is attained by loading the top radiating edge with rhombic shaped stubs and slots. With this configuration the inductive and capacitive reactance of the antenna is changed and multiband operation is achieved. For proof-of concept demonstration, an antenna with the proposed architecture operating in multiband such that operating at mid band 5G frequencies and in the X band is designed. The designed antenna exhibits strong resonances at four frequencies that are 3.34 GHz, 4.61 GHz. 6.01 and 8.02 GHz with peak gains of 6.76 dBi, 6.47 dBi 7.76 dBi and 5.51 dBi, respectively. Also, to investigate performance change simulations were repeated for the antenna with different geometrical parameters. Results show that

the antenna behavior including resonance frequencies and strength of the resonances changes with the geometry of the loading stubs and slots. These changes were deeply investigated with help of a full set of parametric study. Moreover, the designed antenna was manufactured and measurements were obtained. It is found that the measurement results are in good agreement with the simulation results. Furthermore, peak gain variation of the designed antenna with frequency and surface current distribution of the antenna at resonance frequencies were calculated. From peak gain variation it is seen that the antenna gain has a tendency to increase with the frequency. This is an expected result because of the fact that as the frequency increases wavelength decreases and thus the antenna becomes electrically large. On the other hand, in the surface current distribution graphs it is seen that the current density is higher around the stubs and slots on the antenna with respect to other parts. This verifies the design idea of the proposed antenna such that stubs and slots at the radiating edge of the antenna increases current path length and thus forces the antenna to resonate in multi band. A comparison was made between the designed antenna and the antennas exist in literature. It is found that despite its smaller or comparable sizes, the designed antenna exhibits more resonances with higher peak gains than the other antennas reported in literature. In addition to all these features, the most significant novelty is the simple structure of the proposed antenna which enables us to achieve multiband operation without making modifications on the ground plane or adding electronic components. We believe that the proposed model can be a successful candidate for 5G, X band and many other bands by allowing simple modifications with its design.

Supplementary Information The online version contains supplementary material available at https://doi.org/10.1007/s11276-023-03250-7.

Acknowledgements The authors would like to thank Abdullah Gul University Electrical-Electronics Engineering Department for providing antenna fabrication, test and measurement facility.

Declarations

Conflict of Interest The authors declare that they have no conflicts of interest.

References

1. Lee, J., Tejedor, E., Ranta-aho, K., Wang, H., Lee, K. T., Semaan, E., Mohyeldin, E., Song, J., Berglijung, C., & Jung, S. (2018). Spectrum for 5G: global status, Challenges, and Enabling Technologies. *IEEE Communication Magazine*, *56*, 12–18. https://doi.org/10.1109/MCOM.2018.1700818.
2. Kaur, N., Sharma, S., & Kaur, J. (2019). Performance comparison of Evolutionary Algorithms in the design of a hand-pump shape Microstrip Antenna for 5G applications. *Elektronika ir Elektrotechnica*, *25*(5), 31–36. https://doi.org/10.5755/j01.eie.25.5.24353.
3. Alieeldin, A., Huang, Y., Boyes, S. J., Stanley, M., Joseph, S. D., Hua, Q., & Lei, D. (2018). A Triple-Band Dual-Polarized indoor base station antenna for 2G, 3G, 4G and Sub-6 GHz 5G applications. *Ieee Access : Practical Innovations, Open Solutions*, *6*, 49209–49216. https://doi.org/10.1109/ACCESS.2018.2868414.
4. Zhang, Y., Zheng, H., Gao, B., Tang, C., Liu, R., & Wang, M. (2019). A Compact Dual-band Antenna for 5G Application. Cross Strait Quad-Regional Radio Science and Wireless Technology Conference, Taiyuan, China. DOI: https://doi.org/10.1109/CSQRWC.2019.8799291.
5. Ullah, M. H., Mandeep, J. S., Misran, N., Yatim, B., & Islam, M. T. (2014). Design and prototyping of a Compact 2S shaped dual Band Patch Antenna. *Elektronika ir Elektrotechnika*, *20*(1), 92–95. https://doi.org/10.5755/j01.eee.20.1.6171.
6. Pei, J., Wang, A., Gao, S., & Leng, W. (2011). Miniaturized Triple-Band Antenna with a defected ground plane for WLAN/WiMAX applications. *IEEE Antennas and Wireless Propagation Letters*, *10*, 298–301. https://doi.org/10.1109/LAWP.2011.2140090.
7. Patel, R. H., Desai, A., & Upadhyaya, T. K. (2018). An Electrically Small Antenna Using Defected Ground Structure for RFID, GPS and IEEE 802.11 a/b /g /S Applications. *Progress In Electromagnetics Research Letters*, vol. 75, pp. 75–81, DOI:https://doi.org/10.2528/PIERL18021901.
8. Reddy, B. R. S., & Vakula, D. (2015). Compact Zigzag-Shaped-Slit Microstrip Antenna with Circular defected Ground structure for Wireless Applications. *IEEE Antennas and Wireless Propagation Letters*, *14*, 678–681. https://doi.org/10.1109/LAWP.2014.2376984.
9. Liu, W., Wu, C., & Dai, Y. (2011). Design of triple-frequency Microstrip-Fed Monopole Antenna using defected Ground structure. *IEEE Transactions on Antennas and Propagation*, *59*(7), 2457–2463. https://doi.org/10.1109/TAP.2011.2152315.
10. Ali, T., Prasad, K. D., & Biradar, R. C. (2018). A miniaturized slotted Multiband Antenna for Wireless Applications. *Journal of Computational Electronics*, *17*, 1056–1070. https://doi.org/10.1007/s10825-018-1183-z.
11. Hajlaoui, E. A., & Almohaimeed, Z. M. A. (2020). New Electromagnetic Band Gap Antenna for multiple Ultrawide Band Applications. *ISSS Journal of Micro and Smart Systems*, *9*, 109–115. https://doi.org/10.1007/s41683-020-00056-z.
12. Rahman, M. M., Islam, M. S., Wong, H. Y., Alam, T., & Islam, M. T. (2019). Performance analysis of a defected ground-structured antenna loaded with stub-slot for 5G communication. *Sensors (Basel, Switzerland)*, *19*(11), 2634. https://doi.org/10.3390/s19112634.
13. Sharma, M. (2020). Design and Analysis of Multiband Antenna for Wireless Communication. *Wireless Personal Communications*, vol. 114, pp. 1389–1402. https://doi.org/10.1007/s11277-020-07425-9.
14. Jing, J., Pang, J., Lin, H., Qiu, Z., & Liu, C. J. (2020). A Multiband Compact Low-Profile Planar Antenna based on multiple resonant stubs. *Progress In Electromagnetics Research Letters*, *94*, 1–7. https://doi.org/10.2528/PIERL20071104.
15. Mondal, K., Sarkar, P. P., & Sarkar, D. C. (2019). High Gain Triple Band Microstrip Patch Antenna for WLAN, Bluetooth and 5.8 GHz/ISM Band Applications. *Wireless Personal Communications*, vol. 109, pp. 2121–2131. DOI: https://doi.org/10.1007/s11277-019-06671-w.
16. Gupta, M., & Mathur, V. (2018). Multiband Multiple Elliptical Microstrip Patch Antenna with Circular Polarization. *Wireless*

Personal Communication, vol. 102, pp. 355–368. DOI: https://doi.org/10.1007/s11277-018-5843-x.
17. Yoon, J. (2006). Fabrication and Measurement of Modified Spiral-Patch Antenna for Use as a Triple-Band (2.4GHz/5GHz) Antenna. *Microwave and Optical Technology Letters*, vol.48, pp. 1275–1279. DOI: https://doi.org/10.1002/mop.21675.
18. Asnani, V., & Baudha, S. (2019). Triple Band Microstrip Patch Antenna useful for Wi-Fi and WiMAX. *IETE Journal of Research*. https://doi.org/10.1080/03772063.2019.1582365.
19. Sahar, N. M., Islam, M. T., & Misran, N. M. (2015). A reconfigurable Multiband Antenna for RFID and GPS applications. *Elektronika ir Elektrotechnika*, *21*(6), 44–50. https://doi.org/10.5755/j01.eee.21.6.13760.
20. Abdulraheem, Y. I., George, A. O., Abdulkareem, S. A., Husham, J. M., Ramzy, A. A., Raed, A. A., & James, M. N. (2017). Design of Frequency Reconfigurable Multiband Compact Antenna Using Two PIN Diodes for WLAN/WiMAX Applications. *IET Microwaves, Antennas & Propagation*, vol. 11, no. 8, pp. 1098–1105. doi: https://doi.org/10.1049/iet-map.2016.0814.
21. Saroj, A. K., & Ansari, J. A. (2020). A reconfigurable multiband rhombic shaped microstrip antenna for wireless smart applications. *International Journal of RF and Microwave Computer Aided Engineering*, *30*, https://doi.org/10.1002/mmce.22378.
22. Singh, P. P., Goswami, P. K., Sharma, S. K., & Goswami, G. (2020). Frequency Reconfigurable Multiband Antenna for IoT Applications in WLAN, Wi-Max, and C-Band. *Progress In Electromagnetics Research C*, vol. 102, pp. 149–162. DOI:https://doi.org/10.2528/PIERC20022503.
23. Ali, T., Khaleeq, M. M., & Biradar, R. C. (2018). A multiband reconfigurable slot antenna for Wireless Applications. *International Journal of Electronics and Communications*, *84*, 273–280. https://doi.org/10.1016/j.aeue.2017.11.033.
24. Carver, K., & Mink, J. (1981). Microstrip Antenna Technology. *IEEE Transactions on Antennas and Propagation*, *29*(1), 2–24. https://doi.org/10.1109/TAP.1981.1142523.
25. Computer Simulation Technology Microwave Studio (CST MWS), Ver (2016). Framingham, MA, USA, 2016.
26. Deshmukh, A. A., Ankit, G., Harsh, C., Rahil, S., Sneha, S., & Ray, K. P. (2012). Analysis of Stub Loaded Circular Microstrip Antennas. International Conference on Advances in Computing and Communications, Cochin, Kerala. pp. 282–285, DOI: https://doi.org/10.1109/ICACC.2012.65.
27. RT/ Duroid 6002 Datasheet. Retrieved April 02, 2022, from RT/duroid 6002 Laminates Data Sheet (rogerscorp.com)
28. Matin, M. A., & Sayeed, A. I. (2010). A design rule for Inset-Fed rectangular microstrip Patch Antenna. *WSEAS Transactions on Communications*, *9*(1), 63–72.
29. Derneryd, A. (1978). A theoretical investigation of the rectangular microstrip antenna element. *IEEE Transactions on Antennas and Propagation*, *26*(4), 532–535. https://doi.org/10.1109/TAP.1978.1141890.
30. Garg, R., Bhartia, P., Bahl, I. J., & Ittipiboon, A. (2001). *Microstrip Antenna Design Handbook*. Artech House: Norwood.
31. Awaleh, A. A., Dahlan, S. H., & Jenu, M. Z. M. (2014). Equivalent Electrical Lumped Component Modeling of E-shaped Patch Flat Lens Antenna Unit Cell. *IEEE Asia-Pacific Conference on Applied Electromagnetics (APACE)*.

Dr. Baris Gurcan Hakanoglu received his B.S. degree from the Department of Electronics and Communication Engineering at Kocaeli University, Turkey and his M.S. degree from the Department of ElectricalElectronics Engineering at Mersin University, Turkey in 2001 and 2005, respectively. He received his Ph.D. Degree from the Department of Electrical-Electronics Engineering at Erciyes University, Turkey in 2021. His research interests include microstrip antenna design and mobile communication systems.

Dr. Veli Tayfun Kilic received the B.S., M.S., and Ph.D. degrees from Bilkent University, Ankara, Turkey, in 2009, 2011, and 2017, respectively, all in electrical and electronics engineering. In February 2018, he joined Abdullah Gul University, Kayseri, Turkey, where he is currently an Assistant Professor at the Department of Electrical and Electronics Engineering. His research interests include radio frequency systems, near-field and far-field electromagnetic coupling, radio frequency antennas, plasmonic antennas, and radio frequency circuits.

Fatih Altindis received his B.S. degree from Bilkent University, Turkey and his M.S. degree from Abdullah Gul University, Turkey both in Electrical and Electronics Engineering in 2016 and 2018, respectively. He is currently going on with his PhD education in Electrical and Electronics Engineering Department in Abdullah Gul University. His research interests include biomedical image processing, biosignal processing and electronics.

Dr. Mustafa Turkmen is an Associate Professor in the Electrical and Electronics Engineering Department at Erciyes University (Turkey). He received his M.S. and Ph.D. degrees from the Erciyes University, both in Electrical and Electronics Engineering, in 2003 and 2009, respectively. He worked for Boston University as a visiting research assistant professor between 2009 and 2012. His current research interests include nanotechnology, fiber laser systems, metamaterials, plasmonics and their applications in chemical and biological sensing, and optical communication and microwave printed circuits, and patch antennas for wireless communication such as wireless local area network (WLAN), and wireless body area network (WBAN) applications. He is a recipient of the Graduate and Postdoctoral Research Fellowships from The Scientifc and Technological Research Council of Turkey (TUBITAK). Prof. Turkmen is also a member of KUSI Group as the Representative of TR72 Region and City of Kayseri, in the Ministry of Science, Industry and Technology. He is also the Founder of Fotonik Technology Co. Inc.